Self-consistent burnup theory clarifies the universality of the peak structure of COVID-19 pandemics.

Koji Niita (niita@rist.or.jp)
Research Organization for Information Science & Technology, Japan

Research Article

Keywords: SIR model, Self-consistent, COVID-19, Half width, Burnup

Posted Date: June 28th, 2022

DOI: https://doi.org/10.21203/rs.3.rs-1789774/v1

Self-consistent burnup theory clarifies the universality of the peak structure of COVID-19 pandemics.

Koji Niita
Research Organization for Information Science & Technology, Japan

Abstract

The epidemic curve of COVID-19 for the first two years of the pandemic clearly shows a sequential peak structure with a constant half width, despite various levels of preventive measures implemented in many countries and various infection strengths of each coronavirus variant. However, previous epidemic models have not been able to explain this phenomenon. Here we show the mechanism causing this peak structure and the universality of the half width of the peak by means of a self-consistent approach that we have developed. Comparison with the data of all peaks observed in 15 countries strongly suggests that convergence of the epidemic peak is achieved when all susceptible people estimated by the self-consistent approach are infected. This directly causes the universality of the half width. The present approach also provides a method to quantitatively evaluate the effects of various prevention measures and has the ability to predict the peak position and height from the data of the strength of infection in the initial stage of each pandemic peak.

Introduction

Figure 1 shows the daily confirmed cases with a 7-day moving average in Japan (blue line) [1] for the first two years of the COVID-19 pandemic. In the same figure, those of Germany, India, Spain, the United States and the world (red line) [2] are also plotted by scaling these absolute values to approximately fit Japan's value. In Figure 2, we compare the peak shapes of the first wave, the Delta variant, and the Omicron variant for several countries, each of which is scaled to that of Japan (blue lines) in terms of peak position and height.

These figures clearly show two important facts. First, each wave of the COVID-19 variant in each country is rising synchronously throughout the world, and all peaks converge in a certain period of time. The synchronization is understandable because the infectivity of the COVID-19 variant is strong and the movement speed of human flow is very fast worldwide. However, the fact that the peak shape remains even on a global average is not easy to understand.

The second point is the width of each peak. The Figure 2 shows that the half width (FWHM: full width at half maximum) of each peak is almost the same at approximately 30 days, independent of the height of the peaks caused by each Covit-19 variant. Figure 1 shows that the peak height of the Delta variant

is 42 times larger than that of the first wave and that of the Omicron variant is 167 times larger than that of the first wave for the case of Japan. These two facts suggest the existence of a peculiar mechanism of the spread and convergence of COVID-19 infection, which exceeds the influence of various types of preventive measures and various infection strengths of each coronavirus variance. However, previous epidemic models have not been able to explain the mechanism of this phenomenon.

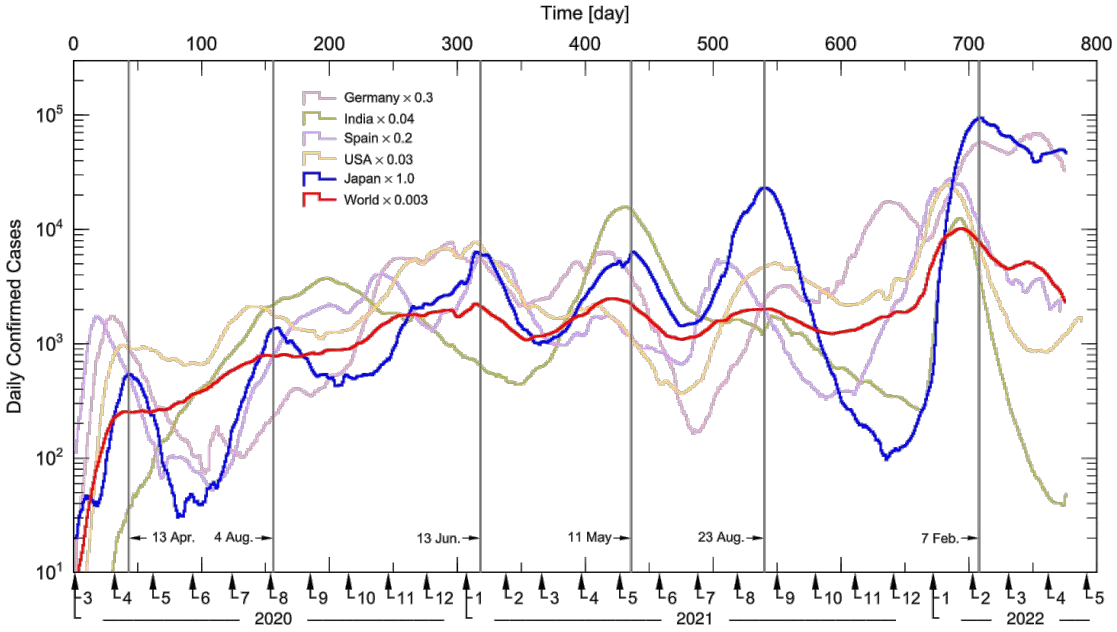

Figure 1 Daily confirmed cases for these two years of the COVID-19 pandemic.

The data of Japan is indicated by blue line. Those of Germany, India, Spain, the United States and the world (red line) are also plotted by scaling these absolute values to approximately fit Japan's value.

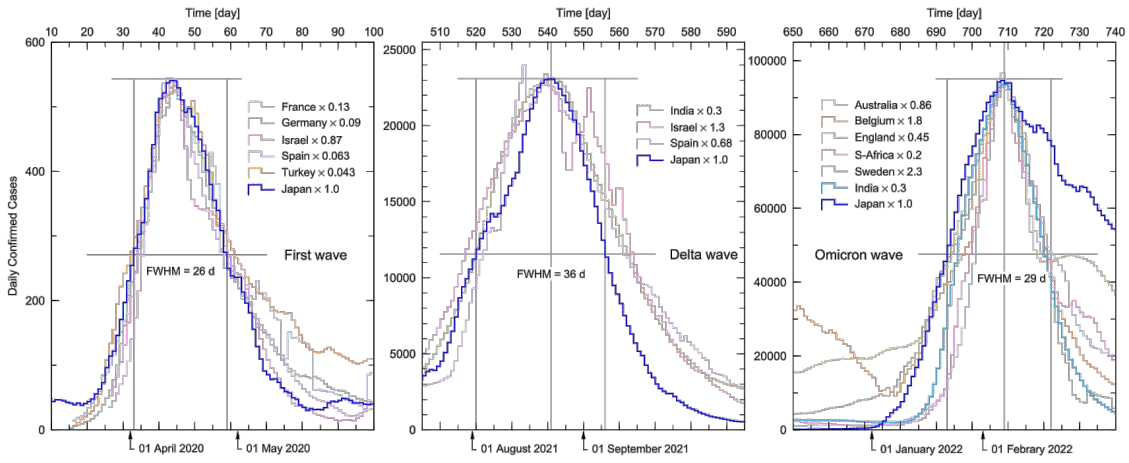

Figure 2 Wave shapes of the first wave, the Delta variant, and the Omicron variant.

The first wave (left-hand), the Delta variant (middle), and the Omicron variant (right-hand) for several countries are shown by scaling them to that of Japan (blue lines) in terms of peak position and height.

Method

Here, we introduce a self-consistent approach, which is an extension of the SIR model [3] (the model and the mathematical framework are described in full detail in the supplementary material). Although the actual numerical solutions have been done in the Monte Carlo method [4] based on the Boltzmann equation for the one-body phase space distribution function, the detail of the self-consistent approach is explained by using the terminology of the SIR model shown below, because the expression is simpler than the explanation by using the Boltzmann equation and because the SIR equations can be straightforwardly derived from the Boltzmann equation.

The simplest expression of the SIR equations for the susceptible $S(t)$, infectious $I(t)$ and recovered $R(t)$ fractions with the transmission coefficient β and the recovered rate λ are given as

$$\begin{cases} \dfrac{dS(t)}{dt} = -\beta S(t)I(t), \\ \dfrac{dI(t)}{dt} = \beta S(t)I(t) - \lambda I(t), \\ \dfrac{dR(t)}{dt} = \lambda I(t). \end{cases} \tag{1}$$

The naive application of this SIR model, in which the total number of people is set as the initial value for susceptible people S_0, is obviously inappropriate, considering that the total number of infected people at the time of the Delta variant in Japan is 920 thousand, which is only 0.7% of the population. At this ratio, the scenario in which a susceptible person is infected and gains immunity, thereby suppressing the spread of infection, does not work at all. This problem is certainly due to the assumption that individual sensitivities are uniform, as many have pointed out [5]. In fact, as Britten *et al*. [6] show, the introduction of age and activity heterogeneities significantly lowers the threshold of herd immunity. Therefore, it is essential to take the heterogeneity of individual susceptibility into account in the theory. However, it is highly uncertain and practically difficult to quantitatively evaluate this nonuniformity and incorporate it into the model, since the heterogeneity of individuals might come from not only the distribution of the susceptibility of individuals, but also the variation in the contact rate by region, and many other elements.

Therefore, we propose another macroscopic approach below, which does not explicitly consider the heterogeneity. We first define the "burnup rate" κ instead of setting S_0 as follows.

$$\kappa = \frac{I_0}{S_0}\ , \tag{2}$$

where I_0 is the cumulative infectious defined by

$$I_0 = \int_0^\infty \beta\, S(t')\, I(t') dt'. \tag{3}$$

The reason for using the terminology "burnup" here is that the mechanism leading to convergence in the SIR model is the reduction of susceptibility due to the progress of infection itself, which is the same as in the general burnup problem. In fact, the equations dealing with the reactor burnup problem have the same structure as those of the SIR model. The word “burnup” is used here because of this similarity.

Next we define the “burnup factor” $\Upsilon(t)$, which is a time-dependent indicator showing the degree of suppression of infection due to the decrease in susceptibility, as follow,

$$\Upsilon(t) = 1.0 - \frac{1}{S_0} \int_0^t \beta\, S(t')\, I(t') dt' \tag{4}$$

By using the burnup factor $\Upsilon(t)$, $S(t)$ is expressed as

$$S(t) = S_0\, \Upsilon(t) \tag{5}$$

The burnup factor $\Upsilon(t)$ changes according to the progress of infection, whose asymptotic value is one at $t = 0$ and $1.0 - \kappa$ for $t = \infty$, that is characterized by the burnup rate κ. The second equation of the SIR model given in Eq.(1) can be rewritten as follows by using the burnup factor $\Upsilon(t)$ defined by Eq.(4).

$$\frac{dI(t)}{dt} = \beta S_0 \Upsilon(t) I(t) - \lambda I(t), \tag{6}$$

We solve the SIR equations (Eq.(1)) with the initial condition (κ, β) instead of (S_0, β). As a result, the SIR equations become equations in which the solution to be obtained includes itself, that is, a so-called self-consistent equation. We solve the self-consistent equations by the sequential imputation method, i.e., repeat the imputation until the solution converges.

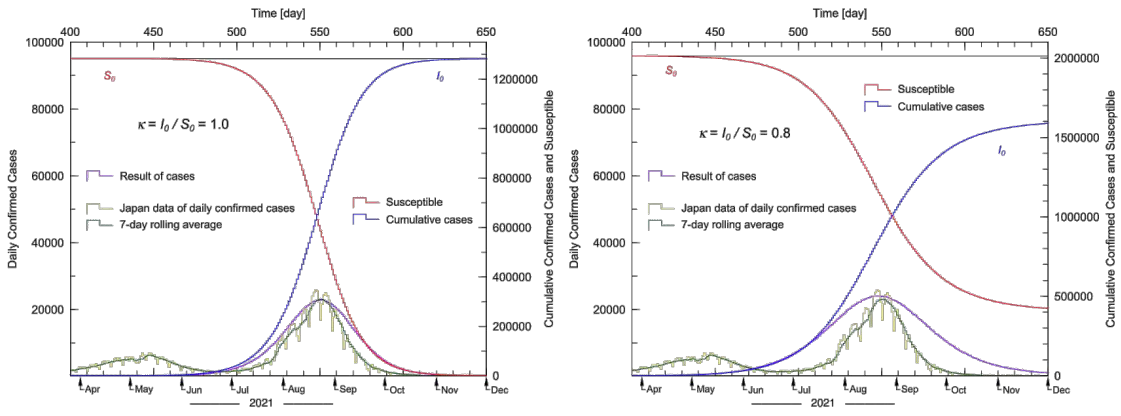

Figure 3 Solutions of the self-consistent equation.

The left-hand side is a result for κ=1.0, and the right-hand side is for κ=0.8.

Figure 3 shows the self-consistent solutions for the initial conditions of κ=1.0 (left graph), κ=0.8 (right graph), and β, which is characterized by the basic reproduction number R_0. The value of R_0 is chosen to reproduce the height of the Delta wave of Japan shown in the same graph. If R_0 is changed with the same κ, the height of the peak is changed but the half width of the peak does not change.

Figure 4 shows the self-consistent solutions with different values of R_0 for κ =1.0 (left graph) and for κ =0.8 (right graph). Both cases denote that the values of R_0 change the height of the peak but do not affect the half width of the peak, which is more strictly shown by the Figure 5. In Figure 5, we scale each peak with different R_0 in Figure 4 to the peak position of the experimental data. These figures clearly show that each result with different R_0 value indicates the same half width for the same κ value.

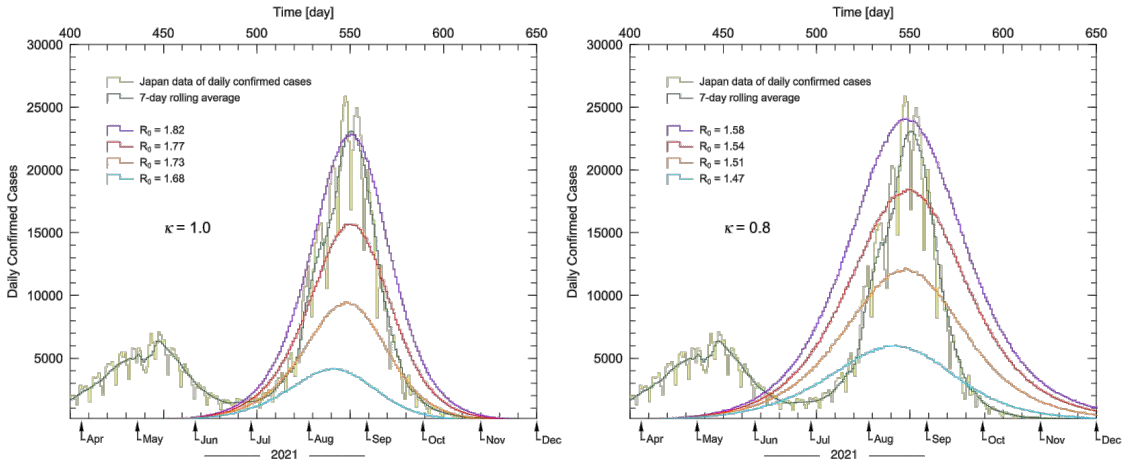

Figure 4 R_0 dependence on the self-consistent solution.

The left-hand side shows the results for κ =1.0, while the right-hand side shows the results for κ =0.8.

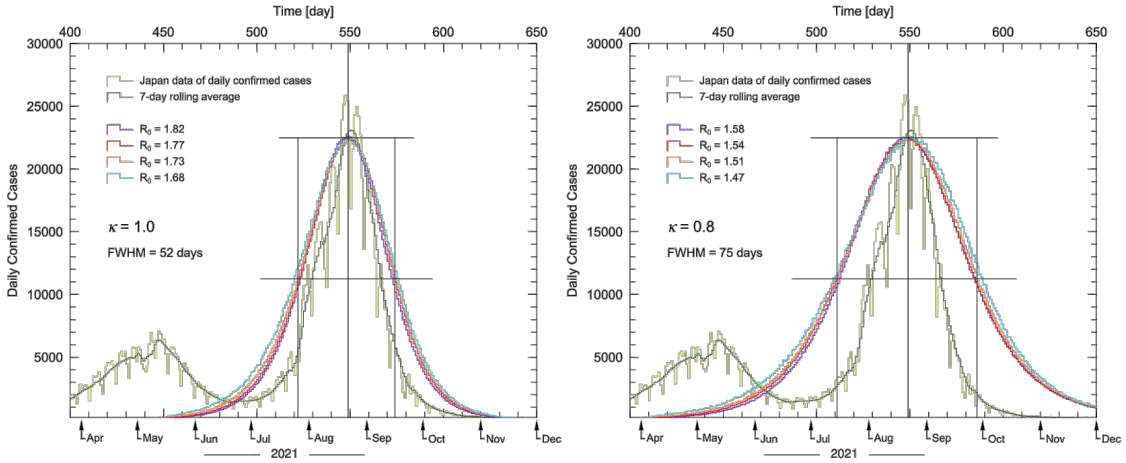

Figure 5 Half width dependence on the different R_0 value.

The left-hand side shows the results for κ =1.0, while the right-hand side shows the results for κ =0.8. Each peak is scaled to the peak position of the experimental data.

These results indicate the unique one-to-one relationship between the burnup rate κ and the half width of the peak and suggest that the shape of the burnup factor $\Upsilon(t)$ (red lines in Figure 3 show $S_0\Upsilon(t)$) might determine the half width of the peak.

Conclusion

This method is applied to all peaks observed in 15 countries. Here, the result of Japan is shown in Figure 6 (the results of the other 14 countries and the details of the methodology and the model are shown in the supplementary material).

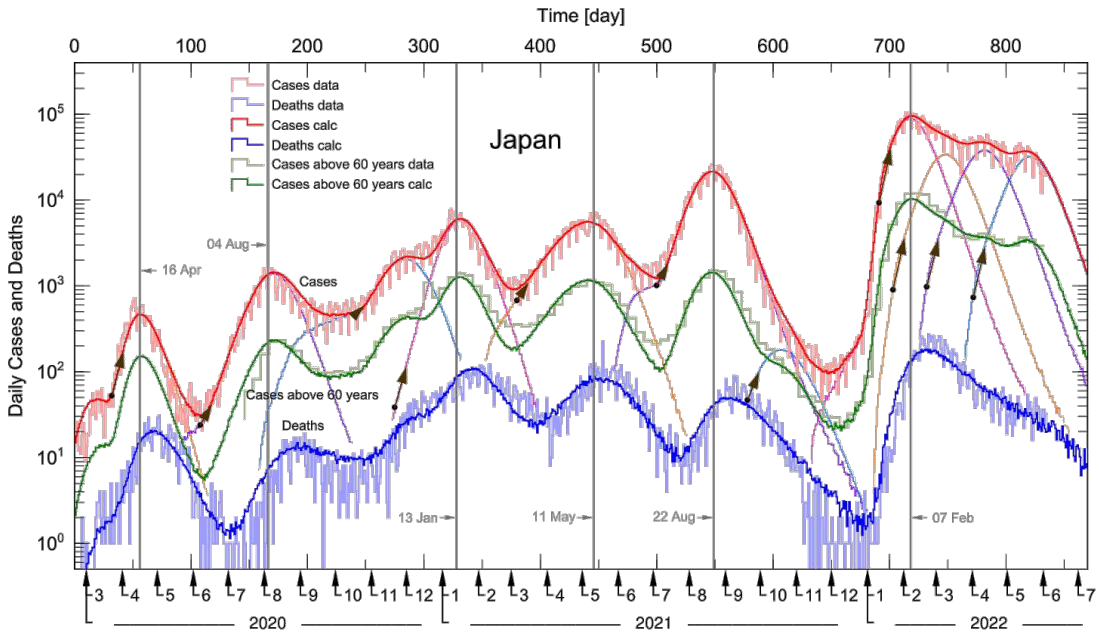

Figure 6 Daily cases (red is all, green is above 60 years old) and deaths of Japan from March 2020 to the present.

For each wave for Japan, the value of R_0 is fixed at the base point of the arrow indicated in Figure 6. After the fixed point, β is not changed and the position and height of the peak are automatically determined by the self-consistent solution. The half width of all waves can be fitted by the condition of κ=1.0. In addition, the comparison with the data of all peaks in another 14 countries also supports the condition of κ=1.0. This suggests that the convergence of the COVID-19 epidemic peak is achieved when all susceptible people evaluated by the self-consistent approach are infected. This might be a reason that the COVID-19 pandemic always shows a constant half width in its epidemic peak, Thus, the half width of the peak does not depend on the strength of the preventive measures or the strength of the infection of each COVID-19 variant. This is an important conclusion obtained by the self-consistent approach, which we call "self-consistent burnup theory", and the condition κ=1.0 is the

"complete burnup condition". It should be noted that the complete burnup condition is not assumed a priori in this theory but is determined by comparing with experimental values.

Applications

This self-consistent approach can also apply to the quantitative evaluation of the effects of various prevention measures. If the effects of the prevent measures are constant in time during the epidemic wave, the self-consistent approach can apply the wave without explicit treatment of the prevent measures, since all information of the effects are already included in the initial condition of β. For the case that the strength of the prevent measures is changed in the period, the information of the time-dependent effects should be included in the simulation in the same time as the burnup factor $\Upsilon(t)$, and the sequential imputation method of the self-consistent approach is performed to reproduce the data. By using this result, we can estimate the effects of the prevention measures by removing the effect from the simulation or by shifting the period of the prevention measures in a virtual way.

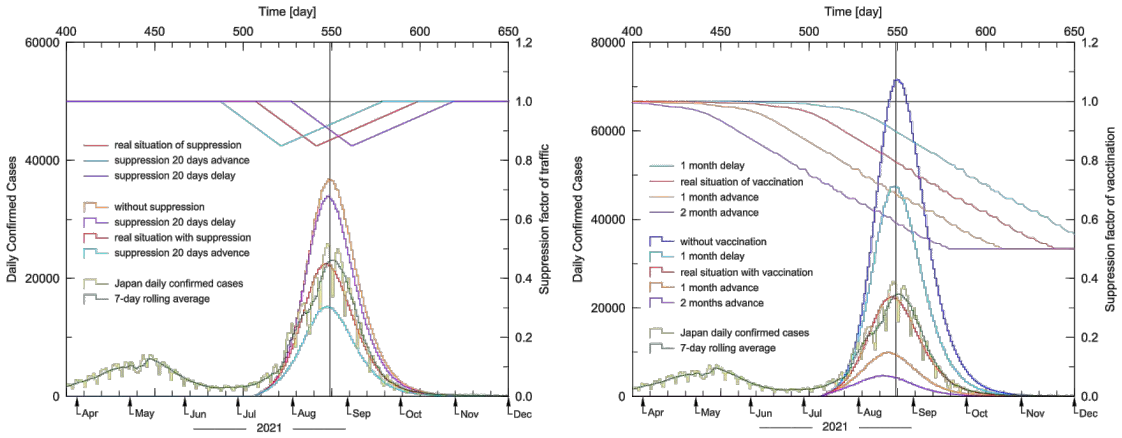

Figure 7 Effects of the preventive measures.
The left graph shows the effects of the suppression of people flow, and the right graph shows the effects of the vaccination.

Figure 7 shows two examples of the estimation of the effects of the preventative measures, the suppression of people flow (left graph) and the vaccination (right graph).

From the data on time changes in the population staying in downtown of Tokyo, we assume the time change of the suppression factor, and the maximum is 15% globally, denoted by the red line in the left graph of Figure 7. Taking this time-dependent suppression factor into the simulation, we perform the self-consistent calculation to reproduce the Delta peak in Japan and obtain the result (red line in the lower part of the left-hand of Figure 7). We then perform the calculations for three cases, by removing the suppression factor (orange line), by sifting it to a 20-day delay (purple line), and shifting it to 20

days advance (cyan line). These results show that the suppression of people flow reduces the infection by 40% for the real situation, 8 % reduction for the 20-days delay case, and 60 % reduction for the 20-days advance case.

These results show that the preventive measures are very effective if they are performed before the peak position but less or almost zero after the peak. It should be noted that the suppression factors at the peak position are almost the same between the delay and advance cases in Figure 7. However, the reduction effect of the delay case is only 8%, while the advance case is 60%. This is because actual infection events peak two weeks before the cases are confirmed. In other words, the preventive measures are expected to be effective up to 2 weeks before the peak of positive individuals.

The next example is the effects of the vaccination (right graph of Figure 7). In the same period of the Delta variant, vaccination has progressed rapidly up to an approximately 70 % vaccination rate in Japan. From these data, we set the time-dependent suppression factor by assuming two things: a 2-week delay in revealing the vaccination effect and 70% efficiency against the infection, shown by the red line in the right graph of Figure 7. As in the previous example, we derive the self-consistent solution (red line), which reproduces the data and four additional results obtained by eliminating the vaccination effect, and shifting the period of the vaccination. These results indicate that the vaccination reduces the infection by 66% for the real situation, 33% reduction for the one month delay case, 85% reduction for the one month advance case, and 92% reduction for the two month advance compared with the no-vaccination case. The conclusions obtained by this example are almost the same as those of the previous example.

Commonly, for both cases, the half width of the peak is not changed by the strength of these prevention measures, which is consistent with the facts observed in Figures 1 and 2.

Validation

Finally, we should mention the predictive performance of the self-consistent approach. Compared with the SIR model, the initial condition κ=1.0 employed in this approach is a strict condition that restricts the available solution space of the SIR model by the condition of the fixed width of the epidemic peak. Due to this condition, the epidemic curve, the peak position and height, can be predicted once we set the initial strength of the transmission coefficient β. Therefore, this condition should be verified from past data, which are partly shown in this paper, and from future predictions.

We started the predictions based on this approach from the beginning of 2022 for 15 countries (full data are shown in the supplementary materials); here, the results of four European countries are shown

in Figure 8.

We predicted the first Omicron peak by using the data up to the end of December 2021, which are shown by purple dashed lines in the graph, and the second Omicron peak by using the data up to 20th of May 2022 shown by the red dashed lines. The purple and red solid lines indicate the calculation results obtained after the data became available. Regarding the height of the peak, it is shown that predicting at a point closer to the peak increases the accuracy, and the smoother the data in the initial stage of the peak, the more accurate the prediction is. In any case, the peak position and width are well predicted by this approach, which strongly suggests that the assumption of κ=1.0 is appropriate.

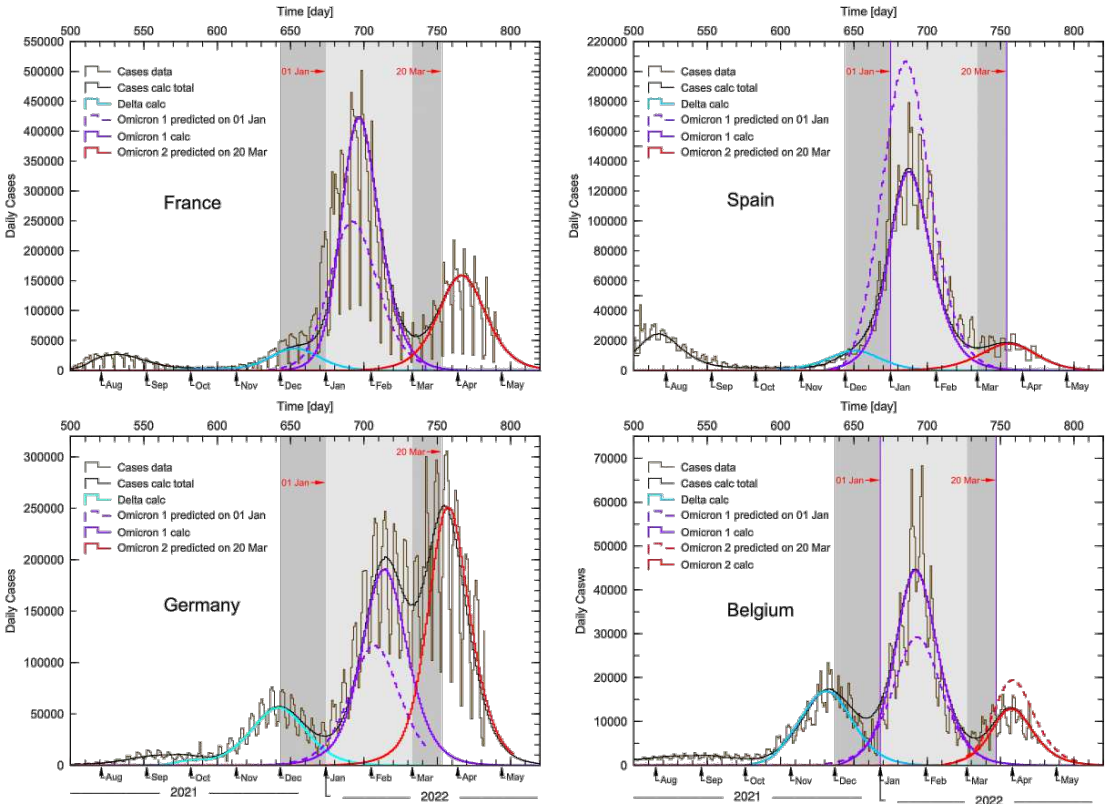

Figure 8 Predictions of the self-consistent approach.

The graphs show the predictions (dashed lines) and the calculated values (full lines) corrected with reference to the data for four European countries from the end of last year to the present.

As shown in Figures 6 and 8, we have divided the epidemic into several peaks and analyzed each component. However, we have not examined the details of the relationship between each peak and real COVID-19 variants, or the interference problem between waves. We assume that all waves are independent. These are the issues to be further investigated in the future

Supplementary Information is available in the online version of the paper.

Acknowledgments

The author thanks Isseki Nagae and Yukitsugu Nakamura for suggesting the intriguing scenario of the "complete burnup condition", which inspired me to do this work.

Author information: Research Organization for Information Science & Technology, Japan

Funding: There are no funding sources to report.

Author contributions: The author performed all tasks.

Competing interests: The author declares no competing interests.

Data availability: The datasets used and/or analysed during the current study available from the corresponding author on reasonable request.

References

[1] Data taken from Ministry of Health, Labour and Welfare Japan; https://www.mhlw.go.jp/stf/covid-19/kokunainohasseijoukyou.html

[2] Data taken from Worldometer; https://www.worldometers.info/coronavirus/

[3] W. O. Kermack, A. G. McKendrick, A contribution to the mathematical theory of epidemics. *Proc. R. Soc. Lond. A*, **115**, 700–721 (1927).

[4] T. Sato, Y. Iwamoto, S. Hashimoto, T. Ogawa, T. Furuta, S. Abe, T. Kai, P.E. Tsai, N. Matsuda, H. Iwase, N. Shigyo, L. Sihver and K. Niita, Features of Particle and Heavy Ion Transport Code System PHITS Version 3.02, *J. Nucl. Sci. Technol.* **55**, 684-690 (2018).

[5] M. G. M. Gomes, R. M. Corder, J. G. King, K. E. Langwig,C. Souto-Maior, J. Carneiro, G. Goncalves, C. Penha-Goncalves,M. U. Ferreira, R. Aguas, Individual variation in susceptibility or exposure to SARS-CoV-2 lowers the herd immunity threshold, *Journal of Theoretical Biology* **540**, 111063 (2022)

[6] T. Britton, F. Ball, P. Trapman, A mathematical model reveals the influence of population heterogeneity on herd immunity to SARS-CoV-2. *Science* **369**, 846–849 (2020).

Supplementary Files

This is a list of supplementary files associated with this preprint. Click to download.

- SCB005S2.pdf